2024 IEEE International Conference on Robotics and Automation (ICRA 2024)
May 13-17, 2024. Yokohama, Japan

Fast Wheeled Driving to Legged Leaping onto a Step in a Leg-Wheel Transformable Robot

Zhi-Ren Chen, Wei-Shun Yu, and Pei-Chun Lin

***Abstract*—The leg-wheel transformable robot has the advantage of smooth, fast, and power-efficient motion on flat terrain and negotiability on rough terrain. This study presents a highly dynamic maneuver of the robot to leap onto a step using its legged form from its original form of wheeled driving, taking full advantage of the rapid switching capabilities of the leg-wheel design of the robot. The robot motion is designed based on a reduced-order model and is planned using an optimization method with multiple constraints. In addition, both position and impedance control strategies are investigated. The proposed strategy is experimentally evaluated. The results show that the robot can leap onto a step higher than itself and then smoothly transition back to the wheeled mode after leaping. The dynamic driving-to-leaping maneuver endows the robot with an alternative and time-efficient approach to negotiate the step obstacles.**

I. Introduction

Legged robots offer numerous advantages when traversing rugged terrains and natural environments, especially those with abrupt height changes, such as steps, or the absence of terrain, such as dip. In contrast, wheel robots offer fast, smooth, and power-efficient motion on flat terrain. Thus, designing a leg-wheel hybrid robot that contains both the legged mode and the wheeled mode acts as one of the popular robot design approaches.

In recent years, various research on leg-wheel hybrid robots has been reported. The leg-wheel hybrid robots come in multiple forms [1]. The first type is articulated-wheeled robots, with wheels added to the legs or joints. These robots can drive the wheels on flat terrain and use their legs or other mechanisms to navigate rough terrain or obstacles. Examples include Hylos [2] and Ascento [3]. The second type is leg-wheel-separated robots. Those robots contain independent sets of wheels and legs, and the robots choose one of them for locomotion, depending on the terrain. The third type is leg-wheel transformable robots, which can change their limb morphology between wheeled and legged forms. Examples nclude Quattroped [4], TurboQuad [5], and the robot utilized in this study, as shown in Fig. 1, also falls into this category [6][7]. No matter the types of hybrid robots, the current studies mainly focus on smooth wheeled motion and quasi-static legged locomotion to negotiate rough terrain. To the best of our knowledge, limited research addresses the dynamic maneuver of the hybrid robot. Thus, one of the significant advantages of the legged robots has yet to be explored.

This study aims to develop a dynamic leaping maneuver for the leg-wheel hybrid robot, as shown in Fig. 1, so the robot can continue to perform fast locomotion even when an obstacle is on its way. As the first attempt, this work focuses on the scenario where the robot initially uses the fast and smooth wheeled motion of the robot on the flat ground, then transforms into a legged mode to leap onto the step obstacle, and then the robot can transform back to the wheeled mode to continue its fast and smooth wheeled motion. In contrast to the traditional approach, where the hybrid robot needs to change into legged mode before the step and then climbs it quasi-statically, the proposed approach has a significant advantage in locomotion speed and motion continuity.

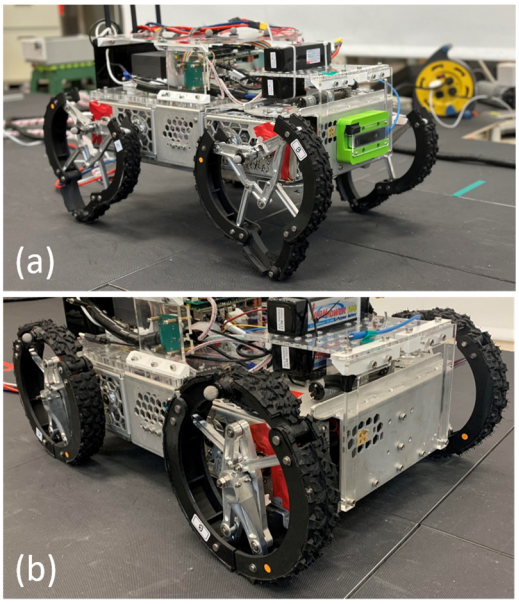

Figure 1. The photo of the leg-wheel transformable robot in legged mode (a) and in wheeled mode (b).

The leg-wheel of the robot has a novel design suitable for dynamic maneuvering [7][8]. It has a leg length of 3.4 times the wheel radius, and it can also fast switch between wheeled and legged modes. Therefore, the fast switching can also induce the leaping behavior of the robot. With the initial fast-moving wheeled mode, the robot leaping onto the step becomes feasible. To the best of our knowledge, no literature is related to the leaping of the hybrid robot. Therefore, the survey of the leaping behavior should extend to a broader range, such as general-legged robots and specialized-design jumping robots.

This work is supported by the National Science and Technology Council, Taiwan, under contract: MOST 110-2221-E-002-111-MY3.

The authors are with the Department of Mechanical Engineering, National Taiwan University (NTU), No.1 Roosevelt Rd. Sec.4, Taipei 106, Taiwan. (Corresponding email: peichunlin@ntu.edu.tw).

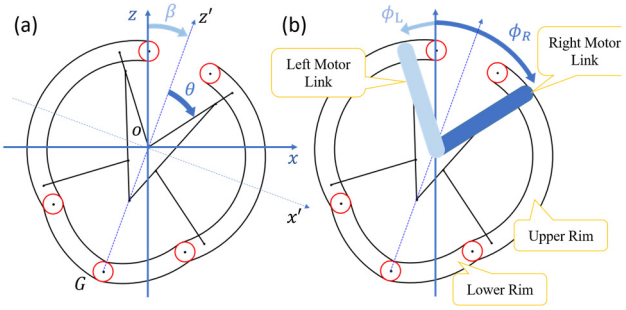

Figure 2. The leg-wheel of the robot: (a) The parameters (θ, β) parametrized the leg-wheel configuration: leg-wheel orientation and leg-wheel length, respectively. (b) The 2-DOF leg-wheel mechansim is driven by the left and right motor links parametrized by (ϕ_L, ϕ_R), regarded as the actuation space.

Jumping is an energy-intensive and complex behavior. ETH [9] had the robot perform hopping on a slope to simulate lunar gravity jumping scenarios, focusing on the robot's repetitive hopping behavior. Using a planar rigid-body model, the RHex-style robot can perform hurdle-like leaping [10]. Previous research [11][12] has simplified robot jumping dynamics using centroidal dynamics [13]. For instance, [11] employed centroidal dynamics and bilevel optimization to plan complex multi-degree-of-freedom robot jumps. Miniature jumping robots often exhibit remarkable jumping capabilities [14][15]. For example, Salto [14] uses springs and unique mechanisms to store energy and perform jumps. Such robots are typically designed specifically for jumping behavior. Some research simplifies a robot's leg into a virtual spring system [16-18]. In [18], a bipedal robot's leg was simplified into a spring system with complex linkages and passive degrees of freedom inspired by the human leg. Optimization algorithms were then used to determine how much torque each actuator needed to approximate the dynamics of the virtual spring. MIT's research on Cheetah 3 [19] demonstrates jumping from a standstill configuration onto a high table using a planar model and optimization technique to find feasible solutions. This study adopts a similar model-based approach followed by optimization to find a feasible leaping solution. Yet because the leaping in this work contains a fast initial forward speed and a unique leg-wheel morphology, the robot's leaping task onto the step has a different executable approach.

The remainder of this paper is organized as follows. Section II introduces the experiment platform, including the robot and half-car platform. Section III describes the leg-wheel dynamic, jump scheduling, and trajectory optimization. The control method is described in Section IV. Section V is the results. Finally, section VI is conclusions and future work.

I. The Leg-Wheel Transformable Robot

The robot utilized in this study is the third generation of the leg-wheel transformable robot developed in the lab. Like the previous two generations, the robot consists of four leg-wheel modules, each with two degrees of freedom (DOFs) moving in the sagittal plane. In addition, a turning DOF is designed for the robot to turn in its wheeled mode.

A. The Leg-wheel of the Robot

Figure 2 shows the leg-wheel of the robot. It is an 11-link mechanism, and the upper and inner two links drive links driven by motors. The motor torque and linkage mechanism are carefully designed to transform the mechanism between the wheeled and legged configurations quickly. The details regarding the leg-wheel design can be found in [8]. The configuration of the leg-wheel is parametrized by two independent parameters (θ, β), where θ controls the distance from the hip joint O to the toe point G (i.e., leg-wheel length) and β determines the angle between the toe point and the body frame (i.e., leg-wheel orientation). The wheel rim comprises four circular arcs, the right/left upper rim and the right/left lower rim, respectively. When $\theta = \theta_0 = 17°$, the two upper rims come into contact with each other, where the leg-wheel is in wheeled configuration. The maximum angle for θ is $\theta_{max} = 160°$, where the leg-wheel has the longest leg configuration.

The desired configuration of the leg-wheel mechanism can be achieved by controlling left and right motor links driven by motors. The configurations of the motor links (ϕ_L, ϕ_R) have one-to-one mapping to the leg-wheel configuration states (θ, β). The relationships between (ϕ_L, ϕ_R) and (θ, β) can be derived as follows:

$$\begin{bmatrix}\phi_R \\ \phi_L\end{bmatrix} = \begin{bmatrix}1 & 1 \\ -1 & 1\end{bmatrix}\begin{bmatrix}\theta \\ \beta\end{bmatrix} + \begin{bmatrix}-1 \\ 1\end{bmatrix}\theta_0 \quad (1)$$

$$\begin{bmatrix}\theta \\ \beta\end{bmatrix} = \frac{1}{2}\begin{bmatrix}1 & -1 \\ 1 & 1\end{bmatrix}\begin{bmatrix}\phi_R \\ \phi_L\end{bmatrix} + \begin{bmatrix}1 \\ 0\end{bmatrix}\theta_0 \quad (2)$$

Each leg-wheel utilizes two brushless DC motors (HT-04, Haitai) to drive the left and right motor links. The motor has a maximum torque of 35 Nm and a maximum rotational speed of 300 rpm, and it also has an embedded planetary gearbox with a reduction ratio of 6:1.

B. The Robot

The robot is composed of four leg-wheels. In addition, it also has an extra DOF to control the front leg-wheels' orientation for turning. When the robot is in wheeled mode, it resembles a four-wheel-drive vehicle. When the robot is in legged mode, it resembles a quadruped where each leg has two DOFs moving in the sagittal plane. The robot in the current morphology does not have AB/AD DOFs. The robot body is constructed from aluminum sheets weighing 26 kg. The inner linkages of the leg-wheel are made of aluminum, and the outer links (i.e., wheel rim) are fabricated using 3D printing with embedded long carbon fiber to increase its strength. The rim is covered with tire treads to increase contact friction. Specifications of the robot are listed in Table I.

C. The Half-Car Platform

To better understand the leaping behavior of the robot, a half-car platform, as shown in Fig. 3, was constructed to evaluate the electromechanical system and mechanism operated in high-dynamic actions. The platform can also test the performance of control methods. The platform consists of two leg-wheel modules representing the front or hind half of the robot, and it is connected to two vertically arranged rails to constrain its motion to vertical motion only. Linear bearings bridge the platform to the rails for smooth and frictionless sliding motion.

II. The Driving-To-Leaping Motion Planning

Leaping is a highly dynamic and complex behavior. Most leaping behavior resides in the forward direction, which keeps the forward momentum while injecting the vertical momentum into the system. Therefore, the driving-to-leaping motion planning focuses on the behaviors only in the 2D sagittal plane.

TABLE I. THE ROBOT SPECIFICATIONS

Parameter	Value	Units
Mass	26	kg
Body Length	0.6	m
Body Height	0.15	m
Body Width	0.33	m
Leg-Wheel Base	0.44	m
Wheel Diameter	0.22	m
Max Leg Length	0.343	m

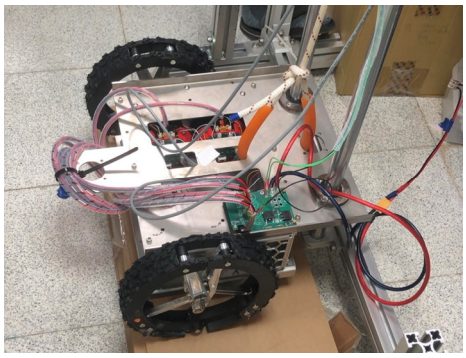

Figure 3. The half-car platform utilized for the initial leaping test.

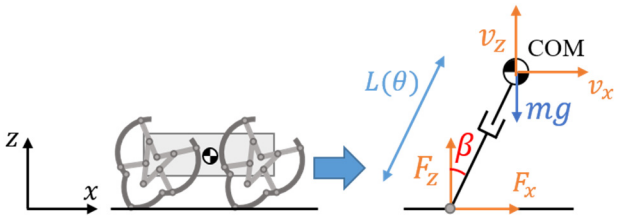

Figure 4. The robot preparing for leaping and its reduced-order single-leg dynamic model.

A. The Reduced-Order Dynamic Model

In general, the legged robots have significant configuration changes during leaping, during which the motor torques quickly transform into ground reaction forces to push the body forward and upward. Owing to the hybrid ground contact conditions of the leg-wheel, the push process may occur in both the rolling and point-contact phases. To simplify the leaping trajectory planning of the robot, a reduced-order single-leg model is adopted, as shown in Fig. 4. The required conditions to make this mapping validate include: (i) The four leg-wheels utilize the same leaping trajectory, so the robot body keeps horizontally. (ii) Following (i), the energy generated from the leg-wheels is mainly for mass but not inertia. (iii) The leg-wheel is a multi-link mechanism which has non-trivial mass. Because the analysis of closed-chain dynamics is highly complex, this study assumes the leg-wheel mass is negligible. Thus, the principle of virtual work can be deployed to deduce the relationship between ground reaction forces and the motor torques, which can be derived using the Jacobian. The equations are as follows:

$$\begin{bmatrix} Fx \\ F_Z \end{bmatrix} = J(\theta, \beta) \begin{bmatrix} \tau_\theta \\ \tau_\beta \end{bmatrix} \tag{3}$$

B. The Four Phases of the Driving to Leaping Motion

This study aims to make the robot leap onto a step obstacle from a high-speed driving motion. The step height is 0.2 meters, close to the wheel diameter. Because the robot has a length of 0.6 meters, the leaping motion involves vertical propulsion and needs to maintain forward momentum so the whole body can fly on the step. Figure 5 shows the robot's driving to leaping motion, which includes four phases: driving, push-off, flight, and landing. The transitions between the consecutive phases can be referred to as leg-wheel transform, liftoff, and touchdown, respectively. In the flight phase, the leg-wheel motion does not alter the body orientation because the leg-wheel mass is ignored.

C. Trajectory Optimization

This study utilizes an optimization algorithm to search for feasible and efficient driving-to-leaping trajectories, optimizing the profiles of the torques of the left and right motor links for force control. During the push-off phase, the objective is to ensure that the robot's center of mass (COM) position and velocity at liftoff are sufficient to clear the obstacle. Owing to the leg-wheel configuration, the direction suitable for actuating forces has a limited range. Therefore, when planning the push-off trajectory, the velocity carried from driving is considered in optimization. If the velocity is low, the vertical take-off velocity V_z is not sufficient for the robot to leap onto the platform.

The optimization focus on the torque command during N discrete time steps, denoted as $\boldsymbol{\tau_{\beta,N}}$, $\boldsymbol{\tau_{\theta,N}}$:

$$\boldsymbol{\tau_{\beta,N}} = [\tau_{\beta,1}, \tau_{\beta,2}, \dots \tau_{\beta,N}] \tag{4}$$

$$\boldsymbol{\tau_{\theta,N}} = [\tau_{\theta,1}, \tau_{\theta,2}, \dots \tau_{\theta,N}] \tag{5}$$

The ground reaction forces, COM position and velocity, denoted as $\boldsymbol{F_N}, \boldsymbol{P_N}, \boldsymbol{V_N}$:

$$\boldsymbol{F_N} = [F_1, F_2, \dots F_N], F_N = \begin{bmatrix} F_{x,N} \\ F_{z,N} \end{bmatrix} \tag{6}$$

$$\boldsymbol{P_N} = [p_1, p_2, \dots p_N], p_N = \begin{bmatrix} p_{x,N} \\ p_{z,N} \end{bmatrix} \tag{7}$$

$$\boldsymbol{V_N} = [v_1, v_2, \dots v_N], v_N = \begin{bmatrix} v_{x,N} \\ v_{z,N} \end{bmatrix} \tag{8}$$

where p_N, v_N can obtained by (3) and discrete equations of motions:

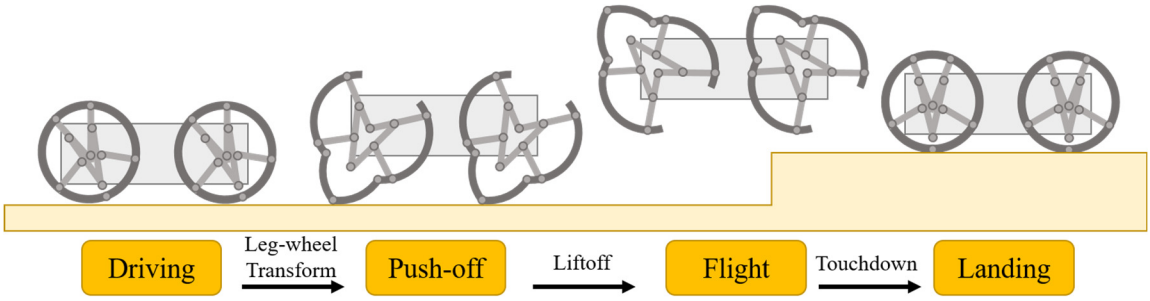

Figure 5. The driving to leaping sequence.

$$v_N = v_{N-1} - \begin{bmatrix}0\\ g\end{bmatrix} T + \begin{bmatrix}F_{x,N-1}\\ F_{z,N-1}\end{bmatrix} \frac{T}{M} \tag{9}$$

$$p_N = p_{N-1} - \begin{bmatrix}0\\ g\end{bmatrix} \frac{T^2}{2} + \begin{bmatrix}F_{x,N-1}\\ F_{z,N-1}\end{bmatrix} \frac{T^2}{2M} \tag{10}$$

The symbol T is the sampling period. The $(p_{x,N}, p_{z,N})$ is related to (θ_N, β_N) Therefore, from p_N, we can get the next timestamp's (θ_N, β_N):

$$\begin{bmatrix}\theta_N\\ \beta_N\end{bmatrix} = \begin{bmatrix} L^{-1}\left(\sqrt{p_{x,N}^2 + p_{z,N}^2}\right) \\ \frac{\pi}{2} - \tan^{-1}\left(\frac{p_{z,N}}{p_{x,N}}\right)\end{bmatrix} \tag{11}$$

where L^{-1} is a look-up table that transforms the leg length to θ.

Because driving-to-leaping behavior is relatively complex, the goal of the cost function is to find feasible solutions while minimizing extreme changes in torque. Because the motor input is ϕ_R, ϕ_L. Calculating cost needs to transform $\boldsymbol{\tau_{\beta,N}}$, $\boldsymbol{\tau_{\theta,N}}$ to $\boldsymbol{\tau_{\phi_R,N}}$, $\boldsymbol{\tau_{\phi_L,N}}$ by (1).The cost function in this study is defined as:

$$\sum C_1\left(\left|\boldsymbol{\tau_{\phi_R,N}}\right|^2 + \left|\boldsymbol{\tau_{\phi_L,N}}\right|^2\right) + C_2\left(\left|\dot{\boldsymbol{\tau}}_{\boldsymbol{\phi_R,N}}\right|^2 + \left|\dot{\boldsymbol{\tau}}_{\boldsymbol{\phi_L,N}}\right|^2\right) \tag{12}$$

The constraints include:

- Leg-wheel angle limit: $|\theta_N| \leq 160°$
- Velocity limits of the motor links:
  $|\dot{\phi}_R| \leq \dot{\phi}_{max}, |\dot{\phi}_L| \leq \dot{\phi}_{max}$
- Joint torque limits: $|\tau_{\beta,N}, \tau_{\theta,N}| \leq \tau_{max}$
- Initial leg-wheel configuration: $\theta_1 = 17°, \beta_1 = 0°$
- Initial COM configuration:
  $v_{x,1} = v_{driving,x}$, $v_{z,1} = 0$, $P_{x,1} = 0$, $P_{z,1} = 0.11$
- Final COM configuration: $v_{x,N} = v_{driving,x}$, $P_{x,N} = 0.6$, $P_{z,N} = 0.36$ (make robot jump about 0.25m obstacle.)
- Friction cone constraint: $|F_{x,N}/F_{z,N}| \leq \mu$

When the robot touches down, the leg-wheel configuration must be configured to pose the toe point G point down. The final COM configuration not only considers whether the position and velocity conditions of the COM at liftoff can move forward by one body length and upward by 0.2m but also considers whether the body's position will collide with obstacles under this scenario and whether there is enough space for the body to touch down on the ground.

If the toe point G experiences slipping during push-off, the β of the leg-wheels will deviate significantly, further affecting the magnitude of Fz. Through testing, it was found that the coefficient of friction with the ground is approximately between 0.5 and 0.7. This study takes the conservative value of 0.5 as the coefficient of friction. During experiments, it was also observed that when the leg-wheels transition from wheeled mode to legged mode for take-off, the motion initiation occurs later than the planned moment. This is because one of the motor links exhibits a dramatic motion direction change. Therefore, it is necessary to advance the leg movement during trajectory planning to compensate for this phenomenon. The experimental data show that the switching time for the motor link is approximately 0.03-0.04 seconds, corresponding to 36-48 degrees if calculated from the rotational speed before take-off. Therefore, in trajectory planning, the leg movement is set to begin 45 degrees before the original trigger.

E. Flight and Landing

Because the motion in the push-off phase is highly dynamic, it is challenging to determine the exact position of the leg-wheels in the flight phase. Therefore, the leg-wheel in flight phase is first closed to a designated configuration to avoid interference between the leg-wheel and the obstacles before switching to the landing trajectory.

During the landing phase, the upper rim is utilized for a touchdown to achieve a smooth landing because this setup tolerates a more extensive range of errors. When planning the landing trajectory using the upper rim, the leg-wheel also rolls to reduce the impact of landing, and the leg-wheel can quickly switch to wheel mode to facilitate obstacle traversal.

TABLE II. THE EXPERIMENTAL LEAPING HEIGHTS (MM) OF THE HALF-CAR PLATFORM

Trajectory	Position control	Impedance control
leaping 150mm, constant torque	65	130
leaping 150mm, optimized torque	50	100
leaping 300mm, constant torque	145	270
leaping 300mm, optimized torque	135	315

To avoid excessive motor actions, the leg-wheel is set to rotate along the same direction among all four phases. Note that in liftoff, the controller transforms from impedance control to position control, and the leg-wheel motor angles increase instantly. If the flight position command directly connects to the ideal jumping trajectory, the experiment shows the motor will reverse severely. Therefore, the position control commands the legs to a specific posture first, then ramped to the "touchdown" position smoothly, and the transition time is calculated based on the optimization results.

III. The Joint Controllers

The overall driving-to-leaping behaviors contain four stages with dynamic characteristics, so different control methods are employed. In the first driving phase, the motors are position-controlled because the required motor is not high, and the wheel should maintain a circular shape. The position control is continuously deployed before the push-off phase to grant the correct leg-wheel posture for lift-off. Once the push-off phase is triggered using motor encoder reading, the impedance control is applied:

$$\boldsymbol{\tau_{\phi_R}} = K_p\left(\boldsymbol{\phi_{R,desire}} - \boldsymbol{\phi_R}\right) + \boldsymbol{\tau_{\phi_{R,desire}}} \quad (13)$$

$$\boldsymbol{\tau_{\phi L}} = K_p\left(\boldsymbol{\phi_{L,desire}} - \boldsymbol{\phi_L}\right) + \boldsymbol{\tau_{\phi_{L,desire}}} \quad (14)$$

where k_p is the proportional gain. The controller doesn't use derivative gains because the estimated angular velocity is not stable in the short duration of usage.

The optimized results reveal that the desired τ and the ideal angles for push-off for the left and right motor links can be obtained and deployed by the impedance control. The optimization sampling frequency is 100 Hz, while the robot's controller operates at 400 Hz. Therefore, the spline interpolation is implemented between the nearby solutions from the optimization results. When the robot operates from lift-off to touchdown where higher precision of linkage positions is required, position control is utilized.

IV. The Experimental Results

A. The Half-Car Experiments

The half-car platform is constrained to move along a 1-DOF vertical motion. By actuating the leg-wheel motors to leap vertically, the results allow us to evaluate the performance of hardware, mechatronics, and controller. The experiments include three kinds of variations: leaping height, torque generation method, and control method. The ideal leaping heights are 150mm and 300 mm, testing the performance of the module for different jumping forces. The two methods of torque generation include a constant torque profile and the optimized torque profile using the described optimization method. As for the controller, the position and impedance controllers are utilized.

Table 2 shows the experimental leaping heights of the half-car platform using the described parameter settings. The results reveal that the impedance control performs better than position control in all settings, and the controller performs better in higher ideal leaping heights. We suspect this phenomenon results from the loss generated in the constrained vertical motion of the platform. In short, the combination of optimized torque profile and impedance control yields the best leaping performance, and this setting is deployed in the following robot driving to leaping experiments.

B. The Driving to Leaping Experiments of the Leg-Wheel Transformable Robot

The motion of the robot in the driving-to-leaping experiments is quantitatively measured using the motion analysis system (VICON) sampling at 500 Hz. Additionally, four 6-axis force plates measure the ground reaction forces generated from the four leg-wheels at a sampling rate of 1000 Hz. The robot drives about 5 meters and then initiates its leaping onto the step of height 0.21 meters. The runway is covered with a rubber pad to increase the friction coefficient between the surface and the leg -wheels.

Figure 6 shows the motion snapshots of the leg-wheel transformable robot in the driving to leaping experiment, and Figure 7 shows the associated quantitative experiment data. Figures 7(a) and 7(b) show that the robot can successfully leap onto a step of height 0.21m. The horizontal displacement of the robot before the leaping indicates the smooth wheel driving motion. Figure 7(c) reveals that the forward velocity of the robot maintains at 2-3 m/s, around 4 body lengths per second. The vertical velocity has a huge increase at the beginning of the leaping, and it decreases to zero when the robot land. The vibrating signals results from the impact vibration between the robot and the step. The lateral velocity has some noises owing to signal differentiation. Figure 7(d) reveals that the roll and yaw maintain around zeros as expected, and the pitch variates around 5 deg. As shown in Figure 7(e)-7(f), the time interval from push-off to landing and the transition to wheel mode took only about 0.4 seconds, an extremely dynamic process. Figure 7(e) shows that the ground reaction forces of four leg-wheels exhibit similar profiles, indicating the synchronized leg-wheel motions. The force profile exhibiting a single compression profile also matches the behavior of the reduced-order model shown in Fig. 4. Figure 7(f) reveals that the empirical motor torques have some delay in comparison to the optimal torque profile, revealing that the motors' acceleration capability is less than expected. We believe a better model which considers loss model (i.e., power conversion, mechanism, etc) would improve the accuracy.

V. Conclusions and Future Work

This study reports the robot's trajectory design and motion control to perform the highly dynamic driving to leaping behavior. The behavior contains four phases: driving, push-off, flight, and landing. Using the optimization method, the motor profile is designed based on the single-leg reduced-order model. As for the trajectory control, the leg-wheel in push-off phase utilizes impedance control, while the other three phases use position control. The half-car platform is built, and its vertical leaping performance is evaluated to

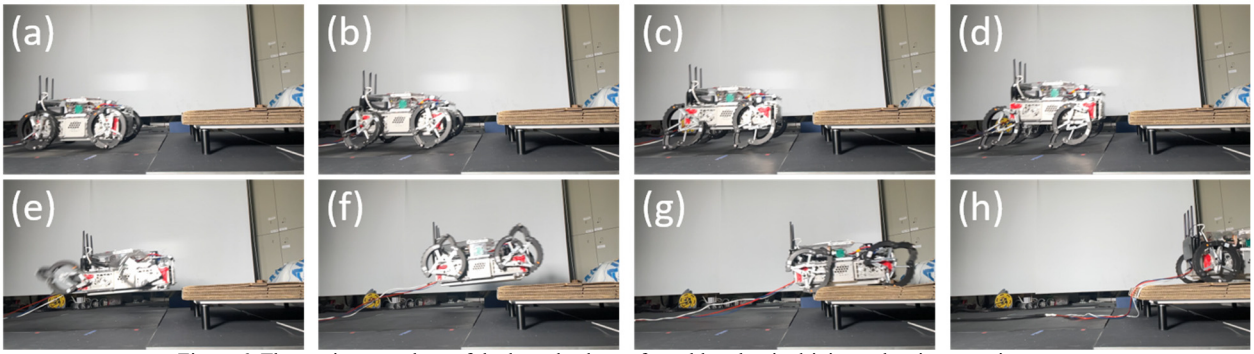

Figure 6. The motion snapshots of the leg-wheel transformable robot in driving to leaping experiment.

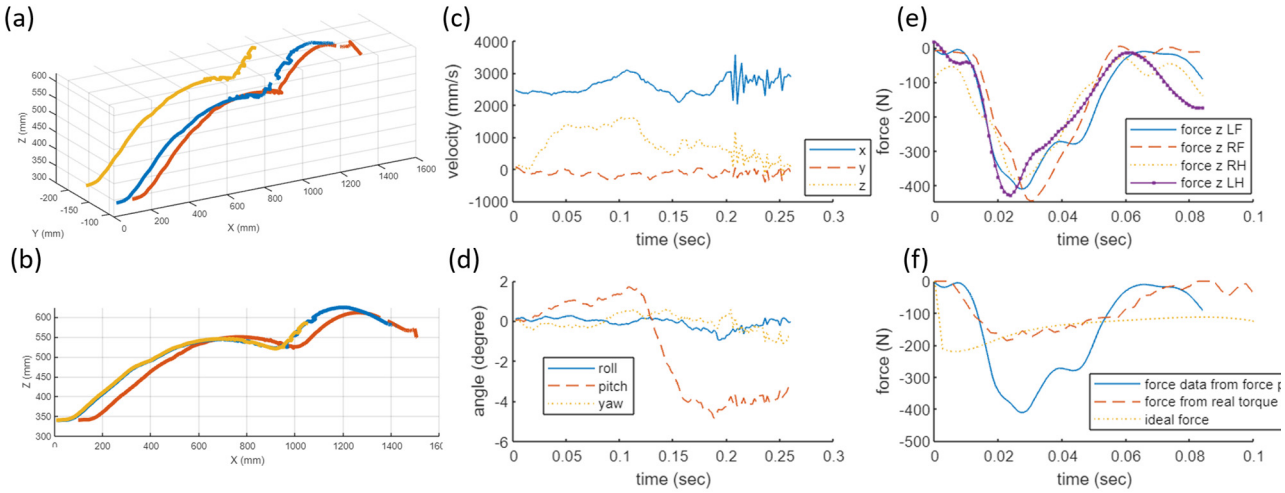

Figure 7. The experimental data of the robot in driving to leaping experiment. The robot displacement in (a) ISO view and (b) side view. The robot's (c) velocity and (d) orientation versus time. (e) The vertical ground reaction forces generated by four leg-wheels and measured by the force plate during the push-off process. The symbols LF, RF, RH, and LH indicate left front, right front, right hind, and left hind legs, respectively. (f) The vertical ground reaction force of the left front leg-wheel as an example. The force curves include the ideal force generated by the optimization algorithm, the force computed from the motor torques with virtual work, and the force measured by the force plate.

validate the capability of the hardware and mechatronics system. Finally, the robot experiment is executed, where the robot can drive at 2.5 m/s and leap onto a step of height 21 cm in 0.4 sec. The consumed time duration is much less than the climbing method, where the robot stops before the step and then climbs up the step. Thus, the developed behavior is advantageous in the case where motion agility is critical.

Our future outlook includes using a more sophisticated model containing the rigid-body maneuver to broaden the possible dynamic maneuver between the wheeled and legged modes. We also plan to add a vision system to fully autonomous the overall process.

REFERENCES

[1] F. Michaud, D. Letourneau, M. Arsenault, Y. Bergeron, R. Cadrin, F. ´ Gagnon, M.-A. Legault, M. Millette, J.-F. Pare, M.-C. Tremblay, P. Lep- ` age, Y. Morin, J. Bisson, and S. Caron, "Multi-modal locomotion robotic platform using leg-track-wheel articulations," Auton. Robots, vol. 18, pp. 137–156, 2005.

[2] Grand, Christophe, Faiz Benamar, and Frédéric Plumet. "Motion kinematics analysis of wheeled–legged rover over 3D surface with posture adaptation." Mechanism and Machine Theory 45.3 (2010): 477-495.

[3] Klemm, Victor, et al. "Ascento: A two-wheeled jumping robot." 2019 International Conference on Robotics and Automation (ICRA). IEEE, 2019.

[4] Chen, Shen-Chiang, et al. "Quattroped: a leg--wheel transformable robot." IEEE/ASME Transactions On Mechatronics 19.2 (2013): 730-742.

[5] Chen, Wei-Hsi, et al. "TurboQuad: A novel leg–wheel transformable robot with smooth and fast behavioral transitions." IEEE Transactions on Robotics 33.5 (2017): 1025-1040.

[6] Huang, Yuan-Cheng, et al. "A Hybrid Impedance and Admittance Control Strategy for a Shape-Transformable Leg-Wheel." 2023 IEEE/ASME International Conference on Advanced Intelligent Mechatronics (AIM). IEEE, 2023.

[7] Liu, Yu-Ju, and Pei-Chun Lin. "Development of a dynamic model of the 11-linkage and closed-chain leg-wheel module." 2022 IEEE/ASME International Conference on Advanced Intelligent Mechatronics (AIM). IEEE, 2022.

[8] Chen, Hsuan-Yu, et al. "Development of a novel leg-wheel module with fast transformation and leaping capability." Mechanism and Machine Theory 163 (2021): 104348.

[9] Kolvenbach, Hendrik, et al. "Towards jumping locomotion for quadruped robots on the moon." 2019 IEEE/RSJ International Conference on Intelligent Robots and Systems (IROS). IEEE, 2019.

[10] Chou, Ya-Cheng, et al. "Model-based development of leaping in a hexapod robot." IEEE Transactions on Robotics 31.1 (2014): 40-54.

[11] Vatavuk, Ivo, and Zdenko Kovačić. "Precise Jump Planning using Centroidal Dynamics based Bilevel Optimization." 2021 IEEE

International Conference on Robotics and Automation (ICRA). IEEE, 2021.
[12] Viereck, Julian, and Ludovic Righetti. "Learning a centroidal motion planner for legged locomotion." 2021 IEEE International Conference on Robotics and Automation (ICRA). IEEE, 2021.
[13] Orin, David E., and Ambarish Goswami. "Centroidal momentum matrix of a humanoid robot: Structure and properties." 2008 IEEE/RSJ International Conference on Intelligent Robots and Systems. IEEE, 2008.
[14] Haldane, Duncan W., Justin K. Yim, and Ronald S. Fearing. "Repetitive extreme-acceleration (14-g) spatial jumping with Salto-1P." 2017 IEEE/RSJ International Conference on Intelligent Robots and Systems (IROS). IEEE, 2017.
[15] Hawkes, Elliot W., et al. "Engineered jumpers overcome biological limits via work multiplication." Nature 604.7907 (2022): 657-661.
[16] Cui, Junwen, et al. "Standing balance maintenance by virtual suspension model control for legged robot." Advances in Mechanical Engineering 12.9 (2020): 1687814020954975.
[17] Hwangbo, Jemin, et al. "Cable-driven actuation for highly dynamic robotic systems." 2018 IEEE/RSJ International Conference on Intelligent Robots and Systems (IROS). IEEE, 2018.
[18] Xiong, Xiaobin, and Aaron D. Ames. "Bipedal hopping: Reduced-order model embedding via optimization-based control." 2018 IEEE/RSJ International Conference on Intelligent Robots and Systems (IROS). IEEE, 2018.
[19] Nguyen, Quan, et al. "Optimized jumping on the mit cheetah 3 robot." 2019 International Conference on Robotics and Automation (ICRA). IEEE, 2019.